Improving Cleanliness of 95CrMo Drill Rod Steel by Slag Refining

LINZHU WANG, SHUFENG YANG, JINGSHE LI, TUO WU, WEI LIU, and JIAZE XIONG

Industrial experiments were performed to improve the cleanliness of 95CrMo drill rod steel by slag refining. Higher steel cleanliness, lower corrosion, and small inclusions were obtained using the optimal slag composition (pctCaO/pctSiO$_2$ = 3.7 to 4, pctCaO/pctAl$_2$O$_3$ = 6 to 8). Layered composite inclusions formed during vacuum decarburizing refining. CaS first precipitated around the spinel and subsequently formed inclusions in which solid CaS-CaO wrapped around the Al$_2$O$_3$-MgO-SiO$_2$-CaO system as the modification and diffusion progressed. The thermodynamic equilibrium between slag and liquid 95CrMo steel at 1873 K (1600 °C) was also studied to understand the effect of slag composition on the oxygen content and absorption capacity for Al$_2$O$_3$. A mathematical model based on an investigation of slag viscosity and the interfacial tension between slag and inclusions was used to predict the size of critical inclusions for different slags. The evolution of typical inclusions is discussed in terms of the study of reactions between slag and steel.

DOI: 10.1007/s11663-015-0481-0

I. INTRODUCTION

DRILL rods, which are extensively used in quarries, open pit mines, and construction sites, are made from hollow steel. They have to bear not only high-frequency peak-value impulse loads but also torsion, bend stress, abrasion, and corrosion from working media such like rock powder.[1] The cleanliness of the molten steel is one of the most important factors influencing the fatigue life and service performance.[2] Stress concentration at the interface between inclusions and the steel substrate, which is affected by the size, morphology, and expansion coefficient difference between the inclusion and steel substrate, is the main cause of fatigue failure.[3] Large, hard, and high melting point inclusions easily initiate micro-voids and cracks at the inclusion/steel interface during hot rolling that can cause fatigue fractures.[4] Strict control of steel cleanliness, including oxygen content and inclusions, therefore, has a very significant influence on improving drill rod quality.[5]

Slag refining is one of the most important and effective ways to evaluate and control steel cleanliness.[6] Slag refining is important to study because of its effects on deoxidation, absorption, and removal of inclusions.[7–9] Low oxygen content and good inclusions can be obtained by improving the physicochemical properties and chemistry of refining slags, such as the value of the pctCaO/pctAl$_2$O$_3$ ratio, slag basicity, fluidity, inclusion/slag interfacial tension, and component activity.[6,10,11]

Many researchers have studied the reactions between slag, inclusions, and molten steel and tried to understand the effect of slag on the evolution of inclusions.[4,12] High melting point spinel and high Al$_2$O$_3$ content inclusions are common with the use of Al as a deoxidizer and in the application of MgO-based refractory materials. These inclusions have a strong impact on the performance and fatigue life of the products.[13] Kim *et al.*[14] proposed that the weight fraction of MgO in the slag is one of the major factors affecting MgO·Al$_2$O$_3$ spinel crystallization. Nishi, Okuyam and Park[15] investigated the equilibrium between Fe-16Cr melts and CaO-Al$_2$O$_3$-MgO slags and found that the relationship between the log of the ratio of mole fraction (X_{MgO}/X_{Al2O3}) of inclusions and the log of the ratio of activities (a_{MgO}/a_{Al2O3}) of the slags exhibited a linear correlation. The absorption ability of slag for Al$_2$O$_3$ was studied by Yoon *et al.*[9] and Bao *et al.*[16] The total oxygen content decreased to 7 to 10 ppm and the absorption ability for Al$_2$O$_3$ was improved by controlling the slag composition to a low melting point region.[16] In a study of the effect of CaO-Al$_2$O$_3$-MgO-CaF$_2$-TiO$_2$ slag composition on the formation of complex oxide inclusions, it was found that the inclusions were mostly located in the "liquid" single phase with lower basicity slags.[10] Jiang and Wang[4] targeted nonmetallic inclusions in the low melting temperature region by changing the slag composition in high-strength alloying steel.

Much research has aimed at improving the quality of different steel grades, such as low-carbon aluminum-killed steel, stainless steel, and bearings,[16–18] by optimizing the composition of refining slags. Few studies of drill rod refining slags have been reported to

LINZHU WANG, Doctoral Student, SHUFENG YANG, Associate Professor, JINGSHE LI, Professor, and TUO WU and WEI LIU, Master's Students, are with the State Key Laboratory of Advanced Metallurgy, University of Science and Technology Beijing, Beijing 100083, China. Contact e-mail: yangshufeng@ustb.edu.cn JIAZE XIONG, Undergraduate Student, is with Shougang Guiyang Special Steel Co., Ltd., Guiyang 550005, Guizhou, China.

Manuscript submitted November 24, 2014.
Article published online October 20, 2015.

date. Owing to the high risk of brittle fractures occurring in high carbon 95CrMo steel, the cleanliness requirement for 95CrMo drill rod is rather strict. In this paper, industrial experiments were conducted to improve the knowledge of this system, and specifically to reducing the oxygen content and number of brittle inclusions, such as those of Al_2O_3 and to decrease the inclusion size, especially for the largest inclusions.

II. EXPERIMENTAL

A. *Production Process*

95CrMo drill rod was produced in a steel plant and the required composition of 95CrMo is shown in Table I according to GB/T 1301-2008. The production process flow comprises treatment of 60 t Consteel by electric arc furnace –ladle furnace (LF) refining, followed by vacuum decarburizing (–VD) refining, and continuous casting of 150 × 150 mm billet. The slag was produced by adding synthetic slag, lime, and other components. The synthetic slag (Table II) was homogenized by premelting, which also facilitated melting. Five types of slag were used, the compositions of which are shown in Table III. Slag A is currently used during the refining process and has low basicity. Slag B has the highest basicity and has the same $pctCaO/pctAl_2O_3$ ratio as slag A. Slags C, D, and E are designed to study the effect of $pctCaO/pctAl_2O_3$ ratio and have medium basicities.

Apart from the slag material, alloys such as aluminum, Si, Mn, and carbon were added as deoxidizers during tapping. High Cr, Mo-Fe, and other alloys were added to meet the steel composition requirements. Heating and soft stirring were conducted to homogenize the molten steel and the slag during the LF refining process. LF refining was completed when the temperature reached about 1873 K (1600 °C) (about 15 minutes). The ladle was transferred for about 20 minutes of vacuum degassing. Soft stirring lasted 6 min and the temperature was about 1803 K (1530 °C) before the steel was transferred to the tundish.

1. *Sampling*

Samples of liquid steel and slag were taken during the refining process for the five types of slag shown in Table IV. The liquid steel was sampled by barrel-type samplers and the slag samples by slag lifters. To study the evolution of inclusions during the production process, full flow sampling was performed for slag B. The sampling steps are shown in Table IV.

2. *Experimental method*

The central parts of the steel specimens were machined into cylinders (Φ5 mm × 100 mm) for total oxygen (TO) measurement and into metallographic samples (15 mm × 15 mm × 15 mm) for compositional analysis and microscopic investigation. Total oxygen content was determined by fusion-infrared absorption. Ca content in steel was analyzed by the ICP-AES method. Other compositions of steel samples were determined by ARL-4460 photoelectric direct reading spectrometry. Inclusions on the cross-sectioned plane of

Table IV. Sampling Plan

No.	Time	Type
Samp. 1	tapping	steel
Samp. 2	middle of LF refining	steel
Samp. 3	end of LF refining	steel and slag
Samp. 4	beginning of VD refining	steel
Samp. 5	end of VD refining	steel

Table I. Chemical Composition of 95CrMo Steel (Weight Percent)

Component	C	Si	Mn	P	S	Cr	Mo	Ni	Cu
Content Range	0.90 to 1.00	0.15 to 0.40	0.15 to 0.40	≤0.025	≤0.025	0.80 to 1.20	0.15 to 0.30	—	≤0.25

Table II. Composition of Synthetic Slag (Weight Percent)

Component	CaO	Al_2O_3	SiO_2	Fe_2O_3	TiO_2	MgO
Typical Content	34.3	40.5	4.7	2.3	2.1	12.8
Range	>32.0	>39.0	<5.5	<3.0	<4.0	>11.0

Table III. Chemical Compositions of Refining Slags

		Chemical Composition (Weight Percent)					
Slag	Remarks	SiO_2	Al_2O_3	CaO	MgO	R	C/A
A	low basicity	23 to 25	7 to 10	58 to 60	6	2.3 to 2.6	6 to 8
B	high basicity	16 to 18	7 to 10	64 to 66	6	3.7 to 4	6 to 8
C	low $pctCaO/pctAl_2O_3$	16 to 18	18 to 20	54 to 56	6	3 to 3.3	2.7 to 3
D	medium $pctCaO/pctAl_2O_3$	16 to 18	13 to 15	54 to 56	6	3 to 3.3	4 to 4.5
E	high $pctCaO/pctAl_2O_3$	18 to 20	10 to 12	58 to 60	6	3 to 3.3	5.5 to 6

the sample were randomly chosen and were analyzed by scanning electron microscopy with energy-dispersive spectrometric detection to get overall and statistical information relating to inclusions, such as their morphology, size, and chemical compositions.

The slag samples were pulverized prior to chemical analysis. Dissolved oxygen in the molten steel was measured using an oxygen probe. The temperature of the molten steel was measured using industrial thermocouples.

The volume fraction of oxide inclusions was estimated from the value of insoluble metal content (M) using the following relationship:

$$f_V = \frac{\rho_{\mathrm{Fe}}}{\rho_{M_xO_y}} \cdot \frac{\mathrm{M}_{M_xO_y}}{x_{M_M}} [\text{ppm insol} \cdot M] \times 10^{-6}, \qquad [1]$$

where ρ_{Fe} is the density of Fe and $\rho_{\mathrm{M}x\mathrm{O}y}$ is the density of the oxide (ρ_{Fe} = 7.8 g/cm^3, ρ_{Al2O3} = 3.97 g/cm^{-3}), $\mathrm{M}_{\mathrm{MxOy}}$ is the molecular weight of $\mathrm{M}_x\mathrm{O}_y$, and [Insol. M] is the insoluble element content (ppm).

III. RESULTS

The slag compositions on completion of LF refining (Sample 3) are shown in Table V. The total SiO_2, Al_2O_3, CaO, and MgO contents comprised greater than 97 pct in all slag compositions and there was little Fe_tO, MnO, TiO_2, or Cr_2O_3 formed during the refining process. The aluminum and oxygen contents are also listed in Table V.

A. *Oxygen Content and Al_2O_3 Volume Fraction in Steel*

The dissolved and total oxygen contents and Al_2O_3 volume fraction in the molten steel for the different types of slags are summarized in Figure 1. The dissolved oxygen content is low in the steel with slag B. This indicates that high basicity has a positive effect on reducing the dissolved oxygen content. The variation of total oxygen content in the molten steels for the different refining slags is consistent with the Al_2O_3 volume fraction. The absorption capacity of slags A and C for Al_2O_3 inclusions is weak. Control of the oxygen content and Al_2O_3 volume fraction in slags B, D, and E is better.

B. *MgO-C Refractory CorrosioN*

The MgO contents in the refining slags after LF refining, shown in Figure 2, reflect the degree of corrosion of the refractory. All slags comprised 6 pct MgO initially. Figure 2 shows that the MgO content in slag B was lower after slagging and the degree of saturation of MgO for high basicity slag is low. The MgO contents of slag A and slag E did not change significantly, indicating that there is neither serious corrosion of the refractory nor reduction of MgO in slag. The refractory corrosion was serious for slags C and D.

C. *Micro-Inclusion Size*

The change of average and maximum inclusions size for the different refining slags after LF refining is shown in Figure 3. Pure MnS and MnS-rich inclusions were

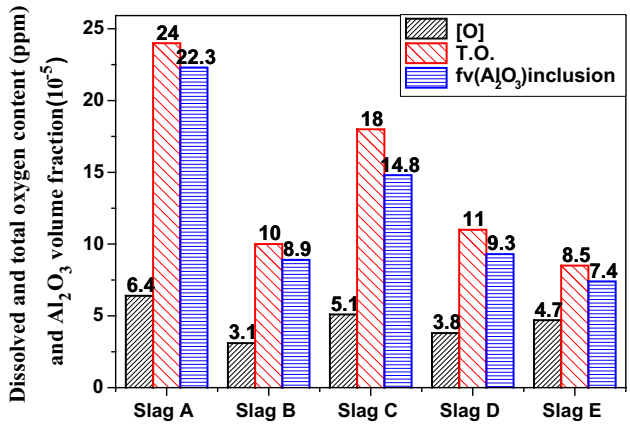

Fig. 1—Cleanliness of different slags after LF refining.

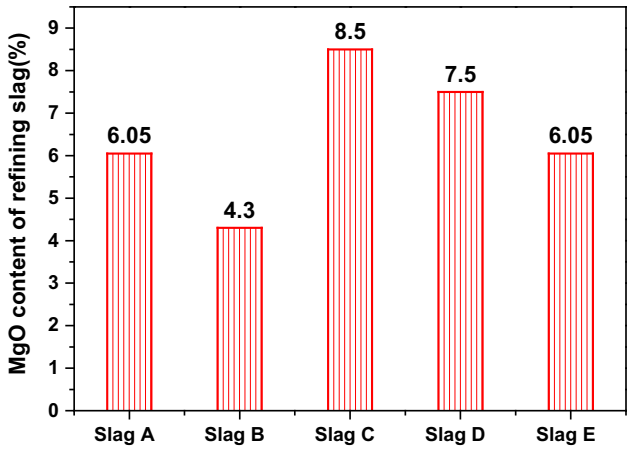

Fig. 2—Effect of refining slag on refractory corrosion.

Table V. Slag Compositions and Aluminum and Oxygen Contents in the Steel After LF Refining (Weight Percent)

	Slag				Steel			
Slag	SiO_2	Al_2O_3	CaO	MgO	Alt	Als	TO	[O]
A	24.15	7.29	59.40	6.05	0.015	0.0090	0.00240	0.00064
B	17.26	8.28	65.83	4.31	0.007	0.0046	0.00100	0.00031
C	16.58	18.51	52.57	8.50	0.009	0.0050	0.00180	0.00051
D	18.95	13.53	58.20	7.51	0.010	0.0075	0.00110	0.00038
E	19.88	11.48	60.05	6.05	0.009	0.0070	0.00085	0.00047

observed in samples 2 and 3. As MnS had not precipitated at refining temperature, they were ignored in the analysis of inclusion size and were not studied in the analysis of micro-inclusion evolution (Paragraph D). The trend for the different slags is the same, indicating that high basicity slags have the strongest effect on the removal of inclusions. The size of inclusions after LF refining was smallest for slag B, with largest inclusion of 4.5 μm and average size of about 3 μm. The inclusion size in slags D and E was second largest. The maximum size of inclusions was 15 μm for slag A, which was the largest observed for the five refining slags investigated.

In conclusion, slag B is the optimal refining slag for 95CrMo drill rod. The improved cleanliness, less refractory corrosion, and smallest-sized inclusions for 95CrMo rod drill were obtained with slag B.

D. *Evolution of Micro-Inclusions*

The micro-inclusions formed during various stages of the refining process were observed in steels made with slag B and analyzed to study their evolution. The average compositional changes of typical micro-inclusions during the refining process are shown in Figure 4. MnS-rich inclusions were observed in samples 2 and 3 which were ignored because they had not precipitated at refining temperature. The average Al_2O_3 content decreased and CaS, CaO, and SiO_2 contents increased. Pure Al_2O_3 inclusions were observed at the beginning of LF refining and some of these transferred into spinel with little precipitated CaS in the outer layer of the inclusion while heating up. Al_2O_3-MgO-CaO-SiO_2-CaS composite inclusions were observed during later stages of LF refining. The composition in the composite inclusions changed during VD refining. Line scanning of typical Al_2O_3-MgO-CaO-SiO_2-CaS inclusions is shown in Figure 5. Layering is obvious, with three layers in typical inclusions. Figure 5 indicates that the inner layer is Al_2O_3-MgO-CaO-SiO_2. A concentration gradient occurred in the outer inclusion layer. The middle and outermost layers were rich in CaO and CaS, respectively. CaO comprised about 50 pct of the middle layer and CaS reached about 60 pct in the outermost layer.

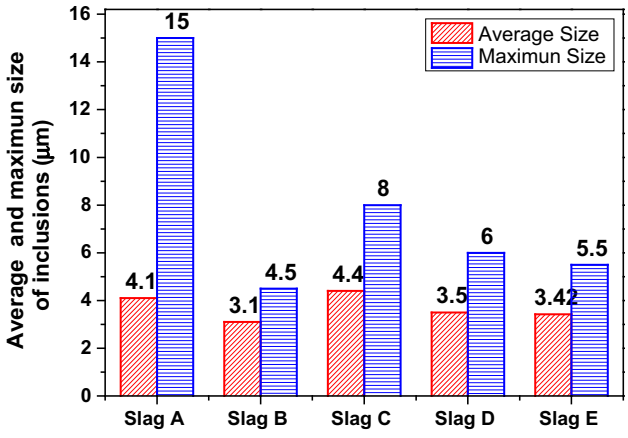

Fig. 3—Average and maximum sizes of micro-inclusions after LF refining.

IV. DISCUSSION

A. *Effect of Slag on Dissolved Oxygen Content*

When equilibrium is reached between oxygen and the Al_2O_3-CaO-MgO-SiO_2 slag, the oxygen content can be expressed as follows:[19]

$$[Si] + [O] = (SiO_2), \qquad [2]$$

$$\Delta G^0 = -576440 + 218.2T \text{ (J/mol)}, \qquad [3]$$

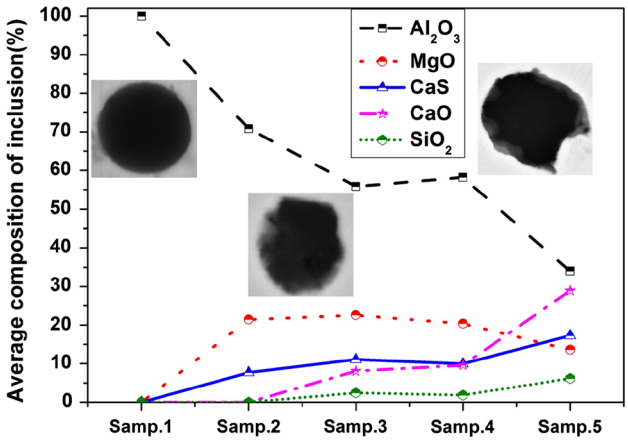

Fig. 4—Evolution of micro-inclusions in slag B during the production process.

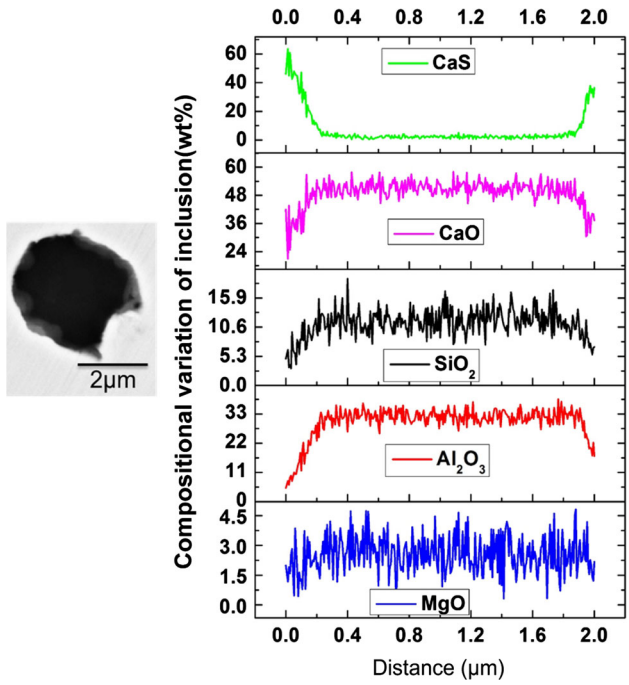

Fig. 5—Line scanning of compositions for a typical Al_2O_3-MgO-CaO-SiO_2-CaS inclusion.

$$[\text{Pct O}] = \left(\frac{a_{SiO_2}}{K \times f_{Si} \times [\text{Si}] \times f_O^2} \right)^{1/2}. \quad [4]$$

Relevant data in Tables VI and VII were substituted into Eq. [4]. Iso-[O] lines representing equilibrium between oxygen and the slag at 1873 K (1600 °C), calculated using Factsage 6.4, are shown in Figure 6, which also shows the measured dissolved oxygen values. The calculated proportion of liquid slag at the end of LF refining is shown in Table VIII. The slag basicity has a significant influence on the equilibrium dissolved oxygen content in the molten steel. The thermodynamic calculation results are shown in Figure 6 and indicate that the equilibrium dissolved oxygen content decreases strongly with increasing slag basicity and with increasing pctCaO/pctAl_2O_3 ratio when the basicity of the refining slag exceeds 2.5. The fluidity of the refining slag has a strong influence on the dynamics of the equilibrium reaction during production. Table VIII indicates that the pctCaO/pctAl_2O_3 ratio affects the fluidity of the refining slag and the proportion of liquid slag increases with decreasing pctCaO/pctAl_2O_3 ratio for these types of slag. Low content oxygen was obtained in steel with liquid slag in the range of 46 to 75 pct.

B. *Effect of Slag on Al_2O_3 Volume Fraction*

The change in Al_2O_3 volume fraction measured during the production of 95CrMo is in good agreement with calculations. Both indicate that a refining slag with low basicity or low pctCaO/pctAl_2O_3 ratio has poor absorption ability for Al_2O_3 inclusions. The absorption ability for Al_2O_3 of refining slags B and E, with high basicity or high pctCaO/pctAl_2O_3 ratio, is strong.

Iso-activities for Al_2O_3 in the SiO_2-CaO-Al_2O_3-MgO 6pct system at 1873 K (1600 °C) were calculated by Factsage 6.4 (Figure 7). The thermodynamic results show that the value of a_{Al2O3} in the liquid region at 1873 K (1600 °C) decreases with increasing slag basicity when the pctCaO/pctAl_2O_3 ratio is fixed and the content of SiO_2 is below 30 pct. The activity of Al_2O_3 in this system increases with decreasing pctCaO/pctAl_2O_3 ratio.

C. *Effect of Slag Viscosity and Interfacial Tension Between the Micro-Inclusion and Slag on Micro-Inclusion Size*

The slag viscosity and interfacial tension between the inclusion and slag have a significant influence on the removal of inclusions from the metal-slag interface.[20,21] Based on the mathematical model of the dynamics of nonmetal inclusions developed by Nakajima and Okamura, Yang *et al.*[8] found that the greater the slag viscosity and interfacial tension, the more difficult is the removal of inclusions. The critical viscosity and interfacial tension for the inclusions of different sizes passing through the slag layer were obtained from the model. Figures 8 and 9 are based on the mathematical model and the data in Tables IX and X and were used to study the influence of slag composition on the critical size of inclusions.

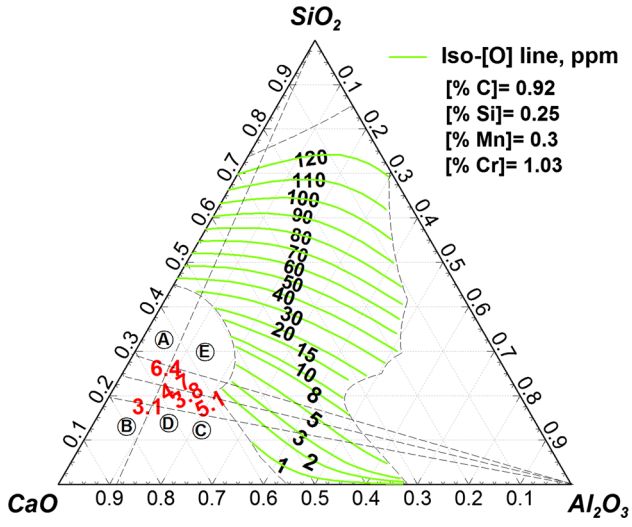

Fig. 6—Iso-[O] lines in CaO-Al_2O_3-SiO_2-MgO6pct at 1873 K (1600 °C).

Table VI. Average Chemical Composition of Molten Steel at the End of LF/Pct

C	Mn	S	P	Si	Ni	Al	Cr	O	N	Mo	Ti	Cu
0.92	0.30	0.01	0.01	0.25	0.043	0.006	1.03	0.0014	0.01	0.2	0.006	0.08

Table VII. Interaction Coefficients of O and Si at 1873 K (1600 °C)

$e_i^j(\rightarrow j)$	C	Mn	S	P	Si	Ni	Als
O	−0.421	−0.021	−0.133	0.07	−0.066	0.006	−1.17
Si	0.18	−0.0146	0.066	0.09	0.103	0.005	0.058
$e_i^j(\rightarrow j)$	Cr	O	N	Mo	Ti	Cu	—
O	−0.055	−0.1743	−0.14	0.005	−1.12	−0.013	—
Si	−0.0003	−0.119	0.092	2.36	1.23	0.0144	—

Table VIII. Proportion of Liquid Slag (Pct)

Slag	A	B	C	D	E
Liquid Slag Percentage	49.4	46.5	96.6	74.9	64

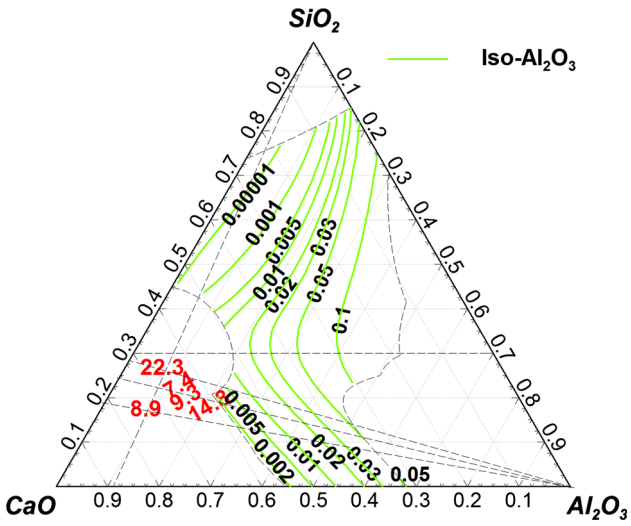

Fig. 7—Iso-activities for Al_2O_3 in CaO- Al_2O_3- SiO_2-MgO6pct at 1873 K (1600 °C).

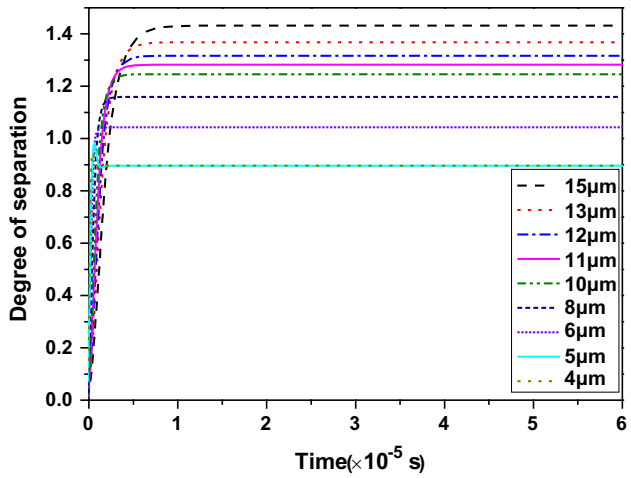

Fig. 8—Change of degree of separation with time for inclusions in slag B.

The viscosities of the five slags calculated by Factsage 6.4 and Zhang's model[22,23] are shown in Table IX. There is some difference between two methods; however, the trend of change in slag viscosity obtained from two models is the same. The average value is used in the mathematical model to reduce error.

There has been little research on a predictive model of interfacial tension between refining slag and inclusions. Based on investigation of the wetting behavior of partially molten CaO-Al_2O_3-SiO_2 and solid Al_2O_3 by Chio and Lee,[24] the interfacial tension between slag D and Al_2O_3 inclusions is about 0.44 N/m without

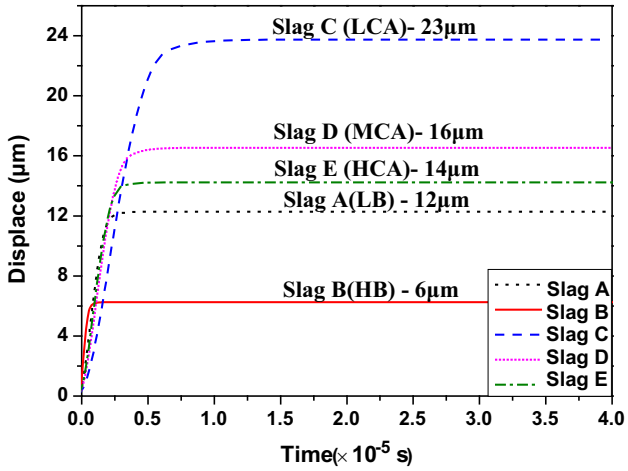

Fig. 9—Change of displacement with time for critical inclusions.

consideration of the presence of MgO. These authors also found that for a slag with a given CaO/SiO_2 ratio, an increase in Al_2O_3 results in an increase in the contact angle and for a given CaO/Al_2O_3 ratio, the variation of the contact angle with SiO_2 content shows a minimum. Therefore, the interfacial tension between other types of slag and Al_2O_3 can be evaluated as given in Table X.

According to the viscosities and interfacial tensions in Tables IX and X, the influence of refining slag on the removal of Al_2O_3 inclusions was calculated based on the mathematical model. The degree of separation is expressed in Eq. [5]:

$$S = \frac{D^*}{D} \qquad [5]$$

where S is the separation degree of inclusion, D^* is the displacement of inclusion (the starting point where the inclusion begins contact with the steel–slag interface), and D is the diameter of the inclusions. When the displacement of an inclusion is greater than the inclusion diameter, the inclusion passes through the slag entirely. In other words, when the degree of separation is greater than 1 and the value remains above 1, the inclusion is removed from the steel. The inclusion cannot be removed when degree of inclusion is smaller than 1.

The degree of separation of 4 to 15 μm inclusions in slag B changed with time as shown in Figure 8. Smaller-sized inclusions exhibited a low degree of separation, *i.e.,* smaller inclusions were more difficult to remove from molten steel. Inclusions larger than 6 μm were rapidly removed and inclusions smaller than 5 μm cannot go into slag B entirely and remain at the slag–steel interface.

Slag composition has a strong effect on the critical inclusion size, which is the size of the smallest inclusion that can be removed from the steel. The change of

Table IX. Viscosities of Refining Slags (Pa·s)

Slag	A	B	C	D	E
Factsage Value	0.064	0.053	0.071	0.064	0.062
Zhang Model Value	0.066	0.04	0.105	0.085	0.079
Average Value	0.065	0.0465	0.088	0.0745	0.0705

Table X. Interfacial Tension Between Refining Slag and Inclusions (N/m)

Slag	A	B	C	D	E
Interfacial Tension	0.425	0.395	0.44	0.43	0.42

displacement for critical inclusions in the five types of slag with time is shown in Figure 9. The order of size of critical inclusion is slag C > slag D > slag E > slag A > slag B. This result is almost consistent with the experimental results. The critical inclusion size is small for a high basicity slag, and for a given basicity, an increase of pctCaO/pctAl_2O_3 ratio in the slag decreases in the size of critical inclusions for 95CrMo refining slag. Inclusions of 6 μm can be removed when the viscosity of refining slag is 0.0465 Pa·s and the interfacial tension is 0.395 N/m.

D. *Effect of Reaction Between Slag and Molten Steel on the Evolution of Typical Inclusions*

The steel–slag reaction has a strong influence on the composition of inclusions. The change of composition and morphology for a typical inclusion during the refining of 95CrMo is shown in Figure 10. The evolution sequence is represented as follows: pure Al_2O_3 → spinel with little precipitated CaS → encapsulated Al_2O_3-MgO-SiO_2-CaO with CaO and CaS → three-layered complex inclusion with a nucleus of Al_2O_3-MgO-SiO_2-CaO. No calcium and sulfur were added deliberately during the industrial experiment in case they effect the results of slag refining (The formation of CaS and MnS in the steel with high Ca and sulfur will effect inclusion evolution and castability of steel which is not the focus of this paper).

Pure Al_2O_3 formed in the molten steel with high Al at the beginning of LF refining when the slag had not started melting.

$$3(MgO)_{\text{refractory or slag}}+2[Al] = (Al_2O_3)_{\text{inclusion}}+3[Mg] \quad [6]$$

$$[Mg] + [O] + (Al_2O_3)_{\text{inclusion}} = (Al_2O_3 \cdot MgO)_{\text{inclusion}} \quad [7]$$

$$(CaO)_{\text{slag}}+[Al] = [Ca] + (Al_2O_3)_{\text{inclusion}} \quad [8]$$

$$[Ca] + [S] \text{ or } [O] = (CaS) \text{ or } (CaO)_{\text{inclusion.}} \quad [9]$$

Spinel was observed in the middle of LF refining because MgO in the slag or refractory was reduced when the slag partially melted during the process of heating up, as reactions [6] and [7] indicate. A certain amount of Ca was detected; this came from the molten slag because no calcium wire was fed and the only source of Ca was the refining slag. The CaO in the molten slag was reduced by Al in the steel by reaction [8]. Although the chemical affinity of calcium for oxygen is higher than that for sulfur, this study shows that calcium reacts with sulfur instead of oxygen when the oxygen activity in liquid steel at 1873 K (1600 °C) is about 19 times lower than sulfur activity.[25] The sulfur content measured in the molten steel was about 100 times that of oxygen, as shown in Table XI. The precipitated composition at the periphery of inclusions is shown in Figure 10(b). Figure 4 indicates that the main calcium reaction product is CaS when the sulfur is high and that the production of solid CaS depends on the [Ca] content.

With increasing [Ca] and a decreasing difference between [O] and [S] during the later stages of LF refining, CaO was observed in the nuclei of inclusions and at the periphery of inclusions containing CaS, as shown in Figure 10(c). This indicates that the difference between the [O] and [S] contents has a strong effect on the production of CaO and CaS, primarily owing to reactions [9] and [10].[26,27] In spite of the transformation of unstable CaS into modified inclusions, the CaS content increases (Figure 4), which indicates that reactions of [9] and [10] take place at the same time:

$$3(CaS)_{\text{inclusion}}+(Al_2O_3)_{\text{inclusion}} = 3(CaO)_{\text{inclusion}}+2[Al] + 3[S] \quad [10]$$

$$x(CaO)_{\text{inclusion}}+y(Al_2O_3)_{\text{inclusion}}+z(SiO_2)_{\text{inclusion}} = (xCaO \cdot yAl_2O_3 \cdot zSiO_2)_{\text{inclusion}} \quad [11]$$

$$[Si] + [O] = (SiO_2)_{\text{inclusion}} \quad [12]$$

Ca content increased obviously during VD refining process as shown in Table XI owing to the reduction reactions, as expressed by Eqs. [8] and [13].[23] Due to

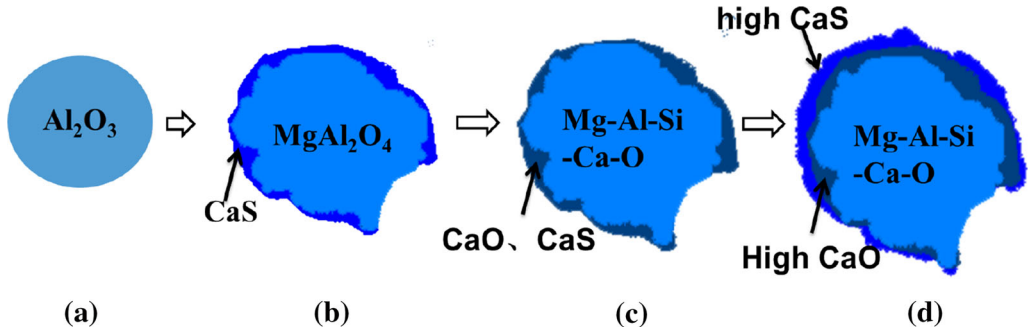

Fig. 10—The evolution of typical inclusion during refining process.

Table XI. Composition of 95CrMo During Refining Process (Weight Percent)

Sample	Als	S	Ca	T.O.	Si
Samp. 2	0.0220	0.0130	<0.0005	0.0013	0.13
Samp. 3	0.0046	0.0067	0.0008	0.0010	0.27
Samp. 5	0.0040	0.0025	0.0014	0.0008	0.31

high content of carbon ($C = 0.96$ pct) in molten steel during VD refining, reaction [13] might be strong which caused increase of CaO, CaS, and SiO_2 in the inclusions and the increase of CaO was more obvious than that of CaS because of the large reduction in sulfur. As the above reaction progressed, the CaS, CaO, and SiO_2 contents were higher in the outer parts of inclusions while lower in the inner parts. The Al_2O_3 and MgO contents were higher in the inner part of inclusions while lower in the outer parts. CaO and SiO_2 diffuse faster than CaS owing to the difference in their chemical affinities with respect to Al_2O_3 and MgO. As modification and diffusion progress, the size of inclusions increases and a layered inclusion structure is formed during VD refining, shown in Figure 10(d), in which the solid CaS-CaO is wrapped around the Al_2O_3-MgO-SiO_2-CaO system. This indicates that with increasing CaO and CaS contents, the inclusions tend to grow and excessively high basicity has a negative effect on reducing size of inclusions. It is, therefore, important to control the CaO content of the slag:

$$(CaO) \text{ or } 1/2(SiO_2)_{slag} + [C] = [Ca] \text{ or } 1/2[Si] + CO. \quad [13]$$

V. SUMMARY AND CONCLUSION

Industrial experiments using 95CrMo drill rod were performed to study the effect of refining slag on the cleanliness of the steel. The equilibrium dissolved oxygen content, absorption capacity of Al_2O_3 inclusions, and effect of slag viscosity and interfacial tension between slag and inclusions on the removal of inclusion were studied to optimize the refining slag for 95CrMo. The results are summarized as follows:

1. Optimal results were obtained with high basicity slag (pctCaO/pctSiO_2 = 3.7 to 4, pctCaO/pctAl_2O_3 = 6 to 8) compared with low (slag A) and medium basicity slags (slags C, D, and E). Under these conditions, the $[O]_{dissolved}$ and TO were, respectively, 3.1 and 10 ppm and the Al_2O_3 volume fraction was 8.9×10^{-9} at the end of LF refining. The largest micro-inclusion was no bigger than 4.5 μm.
2. Thermodynamic results show that dissolved oxygen content decreased and absorption capacity for Al_2O_3 of the refining slag became stronger with high slag basicity and high pctCaO/pctAl_2O_3 ratio.
3. Mathematical modeling indicated that the critical inclusion size is small with a high basicity slag, and for a given basicity, an increase of pctCaO/pctAl_2O_3 ratio in the slag decreases the size of critical inclusions for 95CrMo refining slag.
4. Layered composite inclusions were observed in 95CrMo. CaS first precipitated around spinel first during LF refining. As modification and diffusion progress, a layered inclusion structure gets formed during VD refining in which solid CaS-CaO gets wrapped around the Al_2O_3-MgO-SiO_2-CaO system. The reaction between slag and steel shows that the difference between the [O] and [S] contents significantly affects the production of CaO and CaS. Excessively high basicity also has a negative effect on reducing the size of inclusions.

ACKNOWLEDGMENT

This research is supported by the National Science Foundation of China (Nos. 51474085 and 51304016).

REFERENCES

1. K. McGregor: *The drilling of rock*, Books Ltd., London, 1967.
2. L. Zhang and B.G. Thomas: *ISIJ Int*., 2003, vol. 43, pp. 271–91.
3. P. Juvonen: D.D. Thesis, Helsinki University of Technology, 2004.
4. M. Jiang, X.H. Wang, and W.J. Wang: *Steel Res. Int*., 2010, vol. 81, pp. 759–65.
5. C.J. Cai, S.B. Zheng, J. Chen, Z.Y. Ye, H.G. Li, and J.M. Yang: *Mater. Sci. Forum*, 2014, pp. 289–97.
6. B. Yoon, K. Heo, J. Kim, and H. Sohn: *Ironmak. Steelmak*, 2002, vol. 29, pp. 214–17.
7. S. Chen, M. Jiang, X. He, and X. Wang: *Int. J. Met. Mater*., 2012, vol. 19, pp. 490–98.
8. S. Yang, J. Li, C. Liu, L. Sun, and H. Yang: *Metall. Mater. Trans. B*, 2014, pp. 1–11.
9. M. Valdez, G.S. Shannon, and S. Sridhar: *ISIJ Int*., 2006, vol. 46, pp. 450–57.
10. J.H. Park, S. Lee, and H.R. Gaye: *Metall. Mater. Trans. B*, 2008, vol. 39B, pp. 853–86.
11. H. Ohta and H. Suito: *ISIJ Int*., 1996, vol. 36, pp. 983–90.
12. M. Andersson, M. Hallberg, L. Jonsson, and P.A.R.J.O. Nsson: *Ironmak. Steelmak*., 2002, vol. 29, pp. 224–32.
13. M. Jiang, X. Wang, and J. Pak: *Metall. Mater. Trans. B*, 2014, vol. 45B, pp. 1248–59.
14. J.W. Kim, S.K. Kim, D.S. Kim, Y.D. Lee, and P.K. Yang: *ISIJ Int*., 1996, vol. 36S, pp. 140–43.
15. J.H. Park and D.S. Kim: *Metall. Mater. Trans. B*, 2005, vol. 36B, pp. 495–502.
16. W. Ma, Y. Bao, M. Wang, and D.W. Zhao: *Ironmak. Steelmak*, 2014, vol. 41, pp. 26–30.
17. P. Yan, S. Huang, L. Pandelaers, J. Van Dyck, M. Guo, and B. Blanpain: *Metall. Mater. Trans. B*, 2013, vol. 44B, pp. 1105–19.
18. W. Yang, X. Wang, L. Zhang, Q. Shan, and X. Liu: *Steel Res. Int*., 2013, vol. 84, pp. 473–89.
19. M. Jiang: D.D. Thesis, University of Sicence and Technology Beijing, 2008.
20. J. Strandh, K. Nakajima, R. Eriksson, and P.A.R.J.O. Nsson: *ISIJ Int*., 2005, vol. 45, pp. 1838 47.
21. J. Strandh, K. Nakajima, R. Eriksson, and P.A.R.J.O. Nsson: *ISIJ Int*., 2005, vol. 45, pp. 1597–06.
22. G. Zhang, K. Chou, Q. Xue, and K.C. Mills: *Metall. Mater. Trans. B*, 2012, vol. 43, pp. 64–72.
23. G. Zhang, K. Chou, and K. Mills: *ISIJ Int*., 2012, vol. 52, pp. 355–62.
24. J. Choi and H. Lee: *ISIJ Int*., 2003, vol. 43, pp. 1348–55.
25. T. Lis: *Metalurgija*, 2009, vol. 48, p. 95.
26. N. Verma, P. C. Pistorius, R. J. Fruehan, M. Potter, M. Lind, and S. Story: *Metall. Mater. Trans. B,* 42B, 2011, vol. 42, 711–19.
27. N. Verma, P.C. Pistorius, R.J. Fruehan, M. Potter, M. Lind, and S.R. Story: *Metall. Mater. Trans. B*, 2011, vol. 42B, pp. 720–29.